Colloid Polym Sci (2009) 287:601–608
DOI 10.1007/s00396-009-2010-7

ORIGINAL CONTRIBUTION

Thermoresponsive behavior of charged *N*-isopropylacrylamide-based hydrogels containing gold nanostructures

Linda M. Guiney · Alissa D. Agnello · Julia C. Thomas · Koko Takatori · Nolan T. Flynn

Received: 12 October 2008 / Revised: 24 January 2009 / Accepted: 27 January 2009 / Published online: 19 February 2009

Abstract We report the synthesis of *N*-isopropylacrylamide-based hydrogels containing either an anionic (acrylic acid) or cationic ([2-(acryloyloxy)ethyl]trimethylammonium chloride) co-monomer. These hydrogels were cross-linked with a cleaveable (*N*,*N*′-cystaminebisacrylamide) and/or inert (*N*,*N*′-methylenebisacrylamide) molecule in four combinations. Gold nanostructures were then synthesized within these hydrogel matrices by in situ reduction of a metal ion precursor. The resulting eight nanocomposites and their non-gold-containing (native) analogs were characterized with several analytical methods. UV–visible and infrared spectroscopy revealed differences among the samples based largely on the concentration and identity of cross-linking agent. Equilibrium swelling masses and phase transition behavior point to differences among samples on charge of the hydrogel backbone, cross-linker type, and presence or absence of gold nanostructures. A molecular level explanation for these observations is described.

Keywords Gold nanoparticle · Hydrogel · Responsive · Phase transition

L. M. Guiney · A. D. Agnello · J. C. Thomas · K. Takatori · N. T. Flynn (✉)
Department of Chemistry, Wellesley College,
106 Central Street,
Wellesley, MA 02481-8203, USA
e-mail: nflynn@wellesley.edu

Present Address:
A. D. Agnello
North Seattle Community College,
9600 College Way North,
Seattle, WA 98103-3514, USA

Introduction

Potential applications as sensors [1, 2], actuators [3–5], antibacterial/antimicrobial materials [6, 7], and drug delivery vehicles [8–10] make hydrogel–metal nanostructure composites an important class of materials. One method for making such nanocomposites is synthesizing the metal nanostructure within an existing hydrogel network, a process in which the hydrogel can be considered a "nanoreactor" for the metal nanostructure [6, 11, 12]. Typically, metal ions are introduced by soaking the hydrogel in a solution containing a soluble salt of the target metal. Next, the hydrogel is transferred to a solution containing a chemical reductant such as sodium borohydride. These in situ synthesis methods have recently been reviewed [13].

Among the hydrogels investigated for composite formation with metal nanostructures, those based on *N*-isopropylacrylamide (NIPAm) are the most widely studied. The importance of NIPAm-based materials stems from their environmental sensitivity; NIPAm hydrogels exhibit a thermoresponsive volume phase transition [14]. The nature of the phase transition—its exact temperature and sharpness, for example—is dependent on a number of characteristics of the NIPAm-based hydrogel. Changing porosity [15], synthesis temperature or solvent [16], and cross-linker type and/or concentration [17], along with the incorporation of charged co-monomers [14] are known to have slight to significant influence on the phase transition.

Both gold and silver nanostructures have been created within hydrogels or microgels containing NIPAm [11, 12, 18–20]. In these cases, the composition of the hydrogel influenced the size and morphology of the metal nanostructures created within the hydrogel matrix. Both the concentration and/or type of cross-linker [12, 20] and co-monomer [18] altered metal nanostructure characteristics. In

some cases, the phase transition behavior of the hydrogel was affected by the metal nanostructures [19] whereas in others it was not [11]. More complete understanding of the influence of a hydrogel's parameter on phase behavior of the nanocomposites is necessary to move forward with many of the proposed applications, particularly those in the area of drug delivery.

Our work aims to expand the understanding of thermoresponsive hydrogels containing metal nanostructures by investigating the effect of several variables on the properties of the composites. Specifically, we have investigated the role of charge on the hydrogel backbone by creating cationic ([2-(acryloyloxy)ethyl]trimethylammonium chloride, ATAC) and anionic (acrylic acid, AAc) co-polymers of NIPAm-based hydrogels. We have also explored the importance of cross-linker type and reactivity by using either or both a reactive, disulfide-bridged or an unreactive, methylene-bridged species. We probed the properties of the materials both before and after in situ synthesis of gold nanostructures. The effect on the volumetric phase transition of the composites is also explored because of the importance of this behavior to drug delivery applications. Comparisons to both native hydrogels (those without gold nanostructures) and to hydrogels with only NIPAm are made [19, 20].

Experimental

Materials

NIPAm (Aldrich) was recrystallized from hexane preceding use. *N*,*N*′-cystaminebisacrylamide (CBAm, Sigma), *N,N*′-methylenebisacrylamide (MBAm, Fluka), methanol (MeOH, Aldrich), ammonium persulfate (APS, Aldrich), *N*,*N*,*N*′,*N*′-tetramethylenediamine (TEMED, Sigma), potassium tetrachloroaurate ($KAuCl_4$, Aldrich), sodium borohydride ($NaBH_4$, Aldrich), [2-(acryloyloxy)ethyl]trimethylammonium chloride (ATAC, Aldrich), acrylic acid (AAc, Sigma), and 50 mM pH7.00 phosphate buffer (Fisher Scientific) were used as received. All water used in these experiments was purified to 18 MΩ cm resistivity using a Nanopure Ultrapure Water System with ultra-filtered type I water from Barnstead. Stock solutions of 10.0% *w/v* APS were prepared in water and stored at −10°C.

Hydrogel synthesis

The procedure was adapted from literature methods [19, 20]. NIPAm monomer (0.50 g) was combined with the appropriate volume of AAc or ATAC to yield a 1.0% (wt/wt, relative to the NIPAm) solution. Stock solutions were made for each cross-linking agent. The CBAm stock solution was prepared by dissolving 17.5 mg (0.0684 mmol) CBAm in 0.20 mL methanol, and the stock solution of MBAm was prepared by dissolving 17.5 mg (0.115 mmol) MBAm in 1.0 mL nanopure water. To the NIPAm/AAc or NIPAm/ATAC solution, the appropriate amounts of MBAm and/or CBAm stock solutions were added to reach the desired concentrations. CBAm and MBAm concentrations in these studies were 0.00% MBAm/3.50% CBAm, 1.75% MBAm/1.75% CBAm, 3.50%MBAm/3.50% CBAm, and 3.50% MBAm/0.00% CBAm where the percentage values are weight/weight with respect to the NIPAm mass. From here on, cross-linking concentrations will be given as *X.XX*M/*Y.YY*C with the *X.XX*M and *Y.YY*C referring to the percentage MBAm and CBAm, respectively.

Water was added to raise the total volume of solution to 5.00 mL. The solution was put on ice before adding 25 μL of 10% APS stock solution as an initiator. The solution was flushed with nitrogen for 5 min. Next, 10 μL of TEMED was added to the solution to act as an accelerator.

The hydrogels were polymerized in a gel electrophoresis mold (Bio-Rad) with 0.75 mm spacing at 4°C. Gels were held for 24 h at this temperature, after which the hydrogel slab was cut into disks with a diameter of 8.50 mm. The gels were soaked in 1 L of water for 72 h, changing the water three times. Gels were stored long-term in pH 7 buffer solution.

Nanostructure synthesis

Synthesis of gold nanostructures was performed as described previously, using $KAuCl_4$ as a gold source and $NaBH_4$ as a reductant [19].

Structural characterization

The hydrogel's chemical structures were examined with infrared spectroscopy using a Perkin Elmer Instruments Spectrum One FT-IR spectrophotometer equipped with a Perkin-Elmer Universal ATR sampling accessory. Hydrogels were dried for a minimum of 24 h and were subsequently diced with a razor blade. Spectra were recorded with 64 scans and a resolution of 1.00 cm^{-1} by placing the dried hydrogel over the ATR crystal.

UV–visible spectra were obtained with a Cary Scan 500 UV–vis–NIR spectrophotometer. Spectra were acquired over a range of 400–800 nm with 1.0 nm resolution in a double-beam mode following baseline correction with pH 7.0 phosphate buffer. To ensure that the beam passed through the hydrogel, a brass plate with a 3.0-mm hole was inserted adjacent to the cuvette. The hydrogels were placed in the cuvette so that the hole in the plate was aligned with the center of the hydrogel. Prior to placing in the cuvette,

some hydrogels had to be cut with a razor blade to fit the 1.0-cm pathlength cuvette. Cuvettes containing hydrogels were filled with buffer to avoid dehydration during spectral acquisition. Temperature-step UV–visible spectroscopy experiments were conducted using the same instrument and parameters with the aid of a CARY Varian PCG 150 Water Peltier System, which we have measured to have an uncertainty of ±0.3 °C. Following each step in temperature, the sample was allowed to equilibrate for 20 min prior to recording a spectra. Studies with our system have shown this time is sufficient to achieve equilibrium absorption values for these samples (data not shown).

Phase transition studies

Volumetric phase transition studies were performed by monitoring the temperature-dependent mass of hydrated hydrogels over the temperature range of 25 to ~60 °C. The detailed procedure has been described previously [19] and was modified here only by the use of phosphate buffer as the medium for the hydrogels. All data presented represent the average of a minimum of three separate hydrogel samples for each composition.

Results and discussion

Characterization of hydrogels

Fourier transform infrared (FT-IR) spectroscopy is a valuable technique to confirm polymerization of NIPAm-based hydrogels [21, 22] and evaluate the influence of gold nanoparticle introduction [19]. The technique is particularly useful in our work because of the large number of sample types. Specifically, with four different cross-linker compositions and two co-monomers for both native and gold nanostructure containing hydrogels, a total of 16 distinct samples were analyzed.

We recorded FT-IR spectra of the starting materials—co-monomers (NIPAm, AAc, and ATAC) and cross-linkers (CBAm and MBAm)—which possess the chemical structures shown in Fig. 1a–e, respectively. The FT-IR spectra of the starting materials (data not shown) exhibit the expected peaks for secondary amines (3,300–3,250 cm^{-1}), alkane and alkene groups (3,050 and 2,950 cm^{-1}, respectively), amides (1,650 and 1,550 cm^{-1}), and numerous bands in the fingerprint region below ~1,500 cm^{-1}.

Figure 2 shows FT-IR spectra for both native and gold nanostructure containing 3.50M/0.00C and 0.00M/3.50C of p(NIPAm-*co*-AAc) (a) and p(NIPAm-*co*-ATAC) (b). These spectra contain signatures for the polymerization of NIPAm-based samples [21, 22], differing substantially from the starting materials. Three changes following

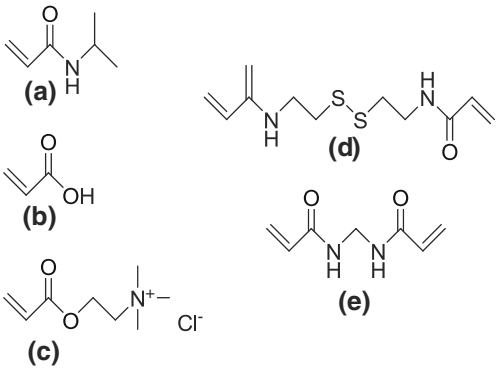

Fig. 1 Chemical structures of NIPAm (**a**), AAc (**b**), ATAC (**c**), CBAm (**d**), and MBAm (**e**)

polymerization are most notable among all samples. First, the 3,600–3,100 cm^{-1} region is dominated by a broad peak characteristic of the bound water observed even in "dried" pNIPAm hydrogels. Second, the amide I and II bands have the expected position and intensity observed for pNIPAm-based materials [21, 22]. Finally, the fingerprint region, particularly below 1,300 cm^{-1}, bares many fewer absorp-

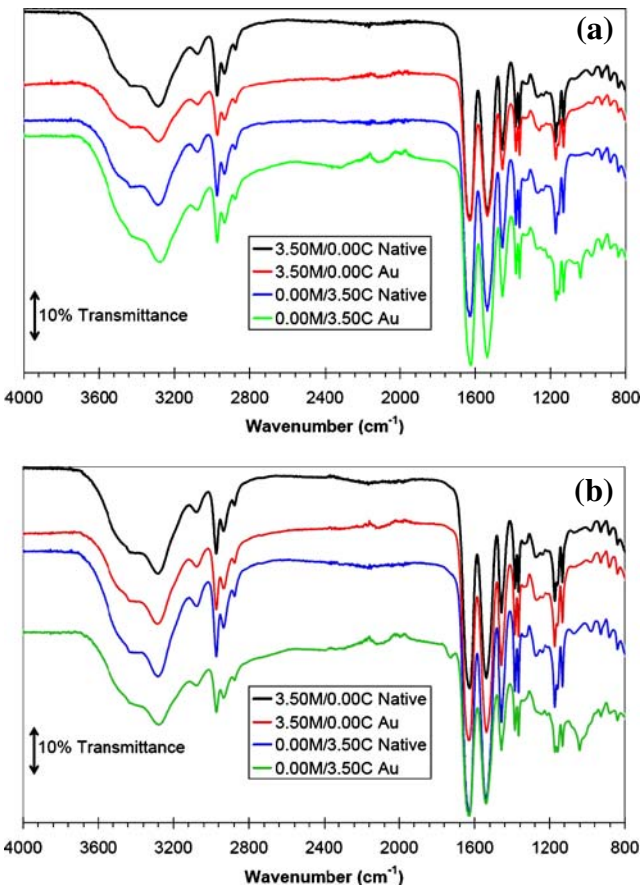

Fig. 2 FT-IR spectra of p(NIPAm-*co*-AAc) (**a**) and p(NIPAm-*co*-ATAC) (**b**). Spectra have been offset along the *y*-axis for clarity and the *double-headed arrow* indicates the scale

tion bands than are observed in spectra from the starting material.

Note that the FT-IR spectra for p(NIPAm-*co*-AAc) (a) and p(NIPAm-*co*-ATAC) (b) both lack any spectral signature indicating the incorporation of the co-monomers. This absence likely results from the low concentration—in each case 1%—of the co-monomer. A second important feature is that the spectra of the CBAm cross-linked hydrogels after gold introduction contain a new band located near 1,040 cm^{-1}. This peak is attributed to the Au^{3+} ions causing oxidation of the disulfide bridge in CBAm to a sulfonate and has been described in detail previously [19]. Notably, this interaction between the Au^{3+} and the disulfide results in the cleavage of cross-links within the hydrogel matrix and concomitant introduction of charge.

All native hydrogels, regardless of co-monomer or cross-linker, were clear and colorless. In situ synthesis of gold nanostructures, however, brought about changes in optical properties that were strongly dependent on the cross-linking agent. Visual inspection shows that gels containing exclusively MBAm are black in color whereas those containing any CBAm were pink to dark red in color. UV–visible spectroscopy enables the elucidation of the origin of the differences among samples.

Figure 3a, b shows the UV–visible spectra for three p(NIPAm-*co*-AAc) and p(NIPAm-*co*-ATAC) hydrogels, respectively, following Au^{3+} introduction and reduction with $NaBH_4$. All spectra possess a peak centered at 520–522 nm, resulting from the surface plasmon resonance of gold nanostructures [23]. Comparing the p(NIPAm-*co*-AAc) hydrogels (Fig. 3a) to the p(NIPAm-*co*-ATAC) hydrogels (Fig. 3b), the former have higher absorbances for a given cross-linking agent. For example, near the peak at 520 nm, the 0.00M/3.50C p(NIPAm-*co*-AAc) hydrogel has an absorbance greater than 1.9 AU whereas the analogous p(NIPAm-*co*-ATAC) hydrogel has an absorbance near 1.2 AU. Similar trends in absorbance are seen for the other two cross-linking compositions: the p(NIPAm-*co*-AAc) hydrogels having a higher absorbance than the analogous p(NIPAm-*co*-ATAC) hydrogels. This difference in absorbance likely results from incorporation of more gold—both Au^{3+} initially and Au nanostructures after reduction—into the anionic p(NIPAm-*co*-AAc) hydrogels. We believe both electrostatics and larger equilibrium swelling, described below, contribute to greater gold incorporation for the p(NIPAm-*co*-AAc) hydrogels.

Previous work by Kim et al. also shows variation of gold nanostructure incorporation by introducing charge into a pNIPAm-based sample [18]. In that work, pure pNIPAm and p(NIPAm-*co*-AAc) nanoparticles were prepared and gold nanostructures were synthesized within the hydrogel particles. Although not a focus of their work, UV–visible spectra presented in the paper show variation in gold incorporation based on changes in the amount of AAc. At a

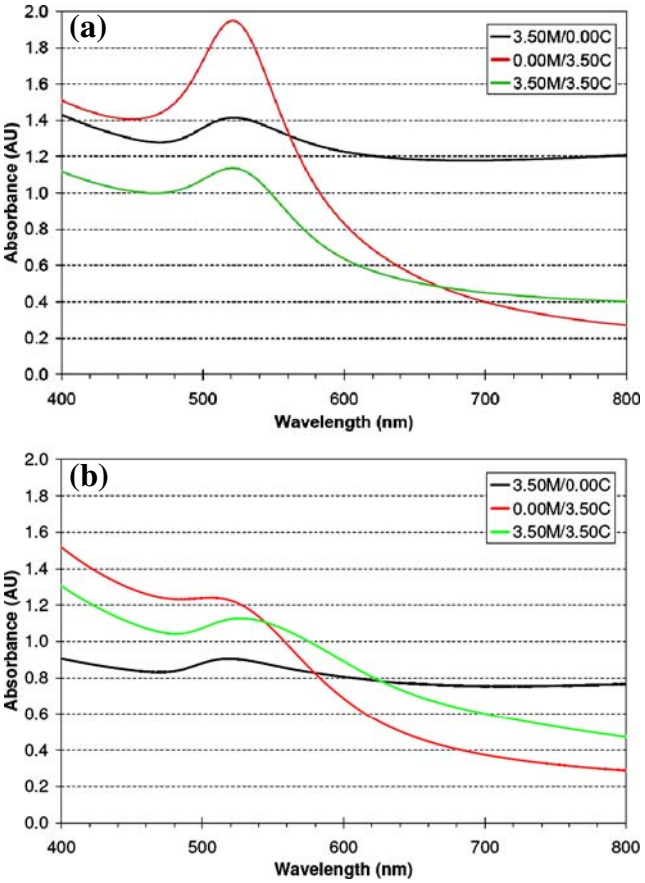

Fig. 3 UV–visible spectra of p(NIPAm-*co*-AAc) (**a**) and p(NIPAm-*co*-ATAC) (**b**) after gold nanostructure synthesis

concentration of 5% AAc, the gold nanostructures exhibit a more intense and sharper surface plasmon band at shorter wavelength compared to pure pNIPAm hydrogel particles. At higher concentrations of AAc, these trends for increased gold incorporation did not continue though that may result from the less reliable preparation and greater aggregation the authors note [18]. Nevertheless, the work by Kim et al. supports our conclusion that charge within a pNIPAm matrix influences the in situ synthesis of gold nanostructures.

The spectra for the three samples—3.50M/0.00C, 0.00M/3.50C, and 3.50M/3.50C—for both hydrogel types exhibit many similar trends. First, the pure CBAm cross-linked hydrogel has the highest absorbance near the peak at 520 nm. Second, for both hydrogel types, the spectra differ most significantly at wavelengths longer than 520 nm. The 3.50M/0.00C sample has a broad absorbance across the 400–800-nm region, whereas the two samples containing 3.50% CBAm have much lower absorbance above 550 nm. Prior work with pNIPAm hydrogels indicates that this difference results from morphological differences between the gold nanostructures formed in the presence and absence of the CBAm cross-linking agent [20]. The black-colored 3.50M/0.00C were found to possess larger, highly aggre-

gated gold nanostructures whereas X.XXM/3.50C hydrogels possessed smaller, well-isolated gold nanostructures. The spectral similarity following gold nanostructure formation of our p(NIPAm-*co*-AAc) hydrogels to the previously investigated pNIPAm hydrogels allows us to conclude that similar differences in gold nanostructure size and aggregation exist in the present work.

The spectral changes caused by heating the hydrogels were also investigated. Figure 4 shows representative spectra from these analyses. Specifically, Fig. 4a contains spectra obtained over the range of 25–48 °C for the native 0.00M/3.50C p(NIPAm-*co*-AAc) hydrogel. All spectra, regardless of temperature, are featureless. As the temperature is increased, the baseline absorbance value increases from near 0.03 AU at 25 °C to slightly greater than 0.25 AU at 48 °C. The increase is likely caused by the collapse of polymer chains, resulting in increases in scattering of light across the visible region [24]. For the 0.00M/3.50C p(NIPAm-*co*-AAc) hydrogel containing gold nanostructures, similar increases in absorbance are seen as the temperature is increased as illustrated by the spectra in Fig. 4b. Here, the change in absorbance across the wavelength range of 400 to 800 nm is again similar despite the presence of the surface plasmon band caused by the presence of the gold nanostructures. Notably, no change in absorbance peak position is seen as the hydrogel begins to collapse.

The increase in absorbance for the native hydrogel (Fig. 4a) is not abrupt, as has been observed for pure p(NIPAm) hydrogels [19], but rather gradual between 34 and 44 °C. Similar behavior is seen for all other hydrogels studied herein, regardless of charge or cross-linking agent (data not shown). This range correlates with differences between the p(NIPAm) and p(NIPAm-*co*-AAc) systems described in the following section. We have not attempted to use the changes in optical properties as a proxy for the phase transition behavior of the hydrogels as is often done with similar systems [14]. With the experimental procedure used in our studies, the hydrogels deswelling may be retarded by interactions of the hydrogel with the cuvette surface. Phase transition behavior is instead probed using equilibrium masses as described below.

The lack of shift in the surface plasmon band for the gold nanostructure-containing hydrogels mimics that observed for the p(NIPAm) analogs with in situ synthesized metal nanostructures [19]. The peak position would be expected to red shift if the nanostructures contacted each other during the deswelling process as a result of the formation of longitudinal surface plasmons within the aggregate [25]. Therefore, it appears the gold nanostructures synthesized within the 0.00M/3.50C p(NIPAm-*co*-AAc) hydrogels are stable and sufficiently isolated to avoid contact even upon collapse of the hydrogel. All other p(NIPAm-*co*-AAc) and p(NIPAm-*co*-ATAC) hydrogels, regardless of the cross-linking agent,

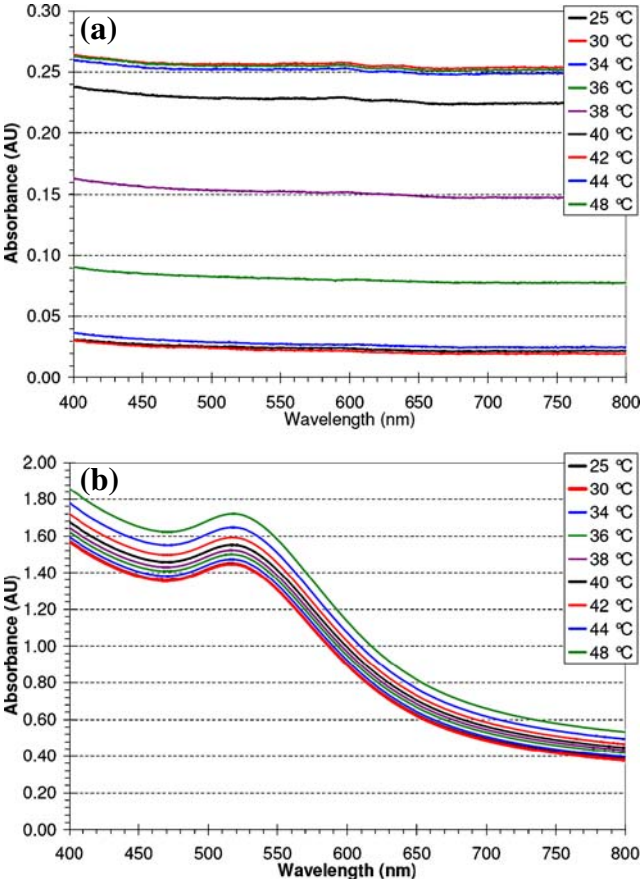

Fig. 4 Temperature-dependent UV–visible spectra for native (**a**) and gold nanostructure-containing (**b**) 0.00M/3.50C p(NIPAm-*co*-AAc). Spectra in the *two panels* are on different absorbance scale because of the substantially lower absorbance of native p(NIPAm-*co*-AAc) hydrogels

showed similar behavior—complete stability of gold nanostructures over the entire temperature range (data not shown). This result contrasts with hydrogel–metal nanostructure composites made using the so-called breathing method of Willner and co-workers in which pre-synthesized nanostructures are introduced into polymerized hydrogels [26].

In addition to the color differences, the in situ synthesis of gold nanostructures causes alteration in the equilibrium swelling of the hydrogels in pH 7 phosphate buffer. Figure 5 shows the average equilibrium swelling mass for the hydrogels studied in this work. All p(NIPAm-*co*-AAc) (Fig. 5a) and p(NIPAm-*co*-ATAC) (Fig. 5b) hydrogels possess significant amounts of water. The dry mass of each gel is approximately 0.005 g, whereas all hydrated masses are greater than 0.030 g.

Several features of the data in Fig. 5 are noteworthy. First, both types of native NIPAm-based co-polymers, shown by the black bars, have the same trend in equilibrium swelling mass with respect to cross-linking agent. Specifically, the 0.00M/3.50C hydrogels are most massive and the 3.50M/

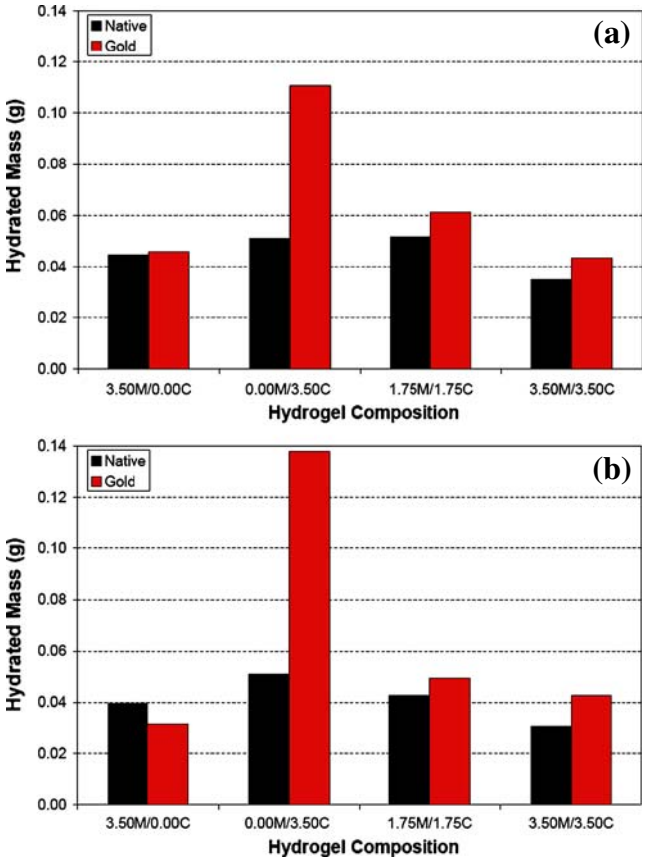

Fig. 5 Equilibrium swelling mass for both p(NIPAm-*co*-AAc) (**a**) and p(NIPAm-*co*-ATAC) (**b**) after immersion in pH7 phosphate buffer. Data are presented for both native and gold nanostructure-containing hydrogels for each of the four cross-linker compositions studied

3.50C hydrogels are the least massive. The high mass of the former may be a result of the ability to reduce the disulfide bridge in CBAm and the low mass of the latter results from the greater total cross-linking in the native 3.50M/3.50C hydrogels than in the other cross-linking systems. Under some conditions, increasing cross-linking density is known to decrease equilibrium swelling volume [17].

A second feature of note is that generally the p(NIPAm-*co*-AAc) native and gold hydrogels possess slightly larger equilibrium swelling masses than the p(NIPAm-*co*-ATAC) analogs. One exception is the 0.00M/3.50C hydrogel containing gold nanostructures for which the ATAC-containing hydrogel has a larger mass than the AAc-containing hydrogel. The difference among hydrogel equilibrium masses possessed by the two co-monomer systems results from several factors. The slightly larger equilibrium masses in the p(NIPAm-*co*-AAc) may result from the expected higher charge within the hydrogel. Because 1% (wt/wt) of co-monomer was added, the AAc is present at more than 2.5 times the concentration of ATAC, AAc having a much lower molar mass (72.06 g/mol compared to 193.67 g/mol for ATAC). Even accounting for incomplete ionization of AAc, which has been seen to possess a pK_a near 4.7 in NIPAm-AAc co-polymers [27], the p(NIPAm-*co*-AAc) will possess greater charge than p(NIPAm-*co*-ATAC) at pH of 7.0. This increased charge is expected to pull in larger quantities of water through the Donnan effect exhibited by polyelectrolyte materials [28].

A third feature is that the introduction of gold causes substantive increases in equilibrium swelling mass for CBAm-containing hydrogels. For example, after gold nanostructure synthesis, the 0.00M/3.50C p(NIPAm-*co*-AAc) sample has a mass increase from 0.051 to 0.111 g and the 0.00M/3.50C p(NIPAm-*co*-ATAC) sample's mass increases by more than a factor of 2.7, from 0.051 to 0.138 g. The increases observed with the 1.75M/1.75C and 3.50M/3.50C hydrogels are more modest but still represent an increase of at least 15% compared to the native hydrated gels. The 3.50M/0.00C hydrogel, which lacks CBAm, however, has a mass 20% lower or negligibly changed for the p(NIPAm-*co*-ATAC) and p(NIPAm-*co*-AAc), respectively, following in situ synthesis of gold nanostructures. The aforementioned interaction of Au^{3+} with the disulfide in CBAm and the reactivity of the latter in general also certainly contribute strongly to the changes in equilibrium mass brought about by exposure to gold ions and subsequent reduction. Oxidation of the disulfide to a sulfonate introduces charge and increases the hydrophilicity of the hydrogel, resulting in increased water uptake. This type of behavior is commonly observed in NIPAm-based hydrogels containing charged co-monomers [14]. The lower cross-linking density after CBAm cleavage is also known to increase equilibrium swelling [29].

Phase transition behavior

NIPAm-based hydrogels exhibit a phase transition upon heating, which has been widely studied. In pure p(NIPAm) hydrogels, this transition occurs near 32 °C and exhibits some dependence on cross-linker concentration [30]. Previously, the phase transition behavior of p(NIPAm) hydrogels with CBAm and/or MBAm as cross-linkers has been reported both with and without gold nanostructures present [19]. The native p(NIPAm) hydrogels, regardless of cross-linker identity or concentration, exhibited similar behavior with a sharp drop in mass by 35 °C. Following gold nanostructure synthesis, however, differences were observed among hydrogels possessing different cross-linking. Specifically, hydrogels containing any CBAm had phase transition temperatures of 5 to 8 °C higher than their native analogs. On the other hand, the 3.50M/0.00C p(NIPAm) hydrogels containing gold nanostructures underwent a phase transition identical to their native precursors.

Figure 6a shows the phase transition behavior for the p(NIPAm-*co*-AAc) hydrogels before (solid symbols and

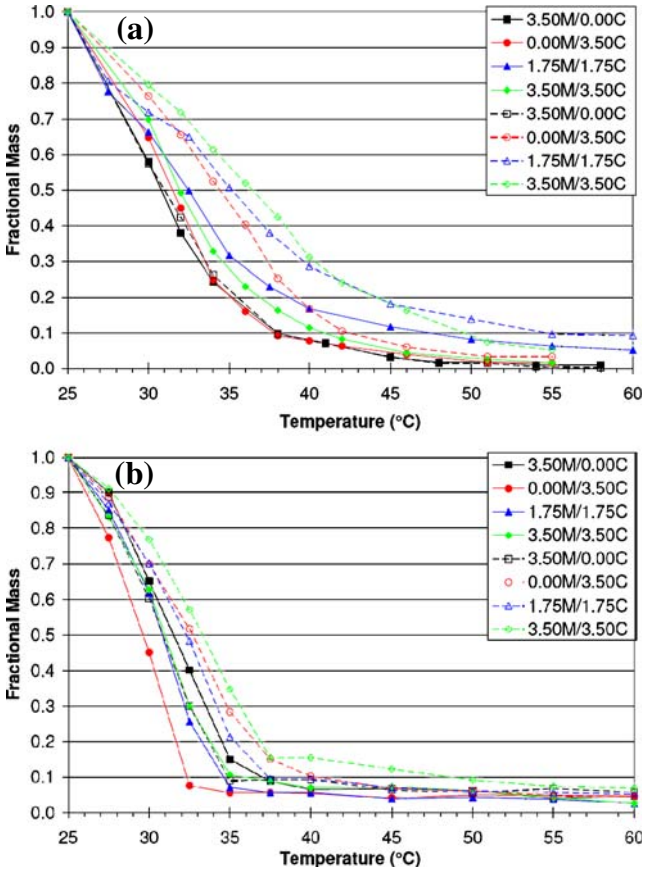

Fig. 6 Phase transition data for p(NIPAm-*co*-AAc) (**a**) and p(NIPAm-*co*-ATAC) (**b**)

lines) and after (open symbols and dashed lines) introduction of gold nanostructures. Figure 6b contains the analogous data for the p(NIPAm-*co*-ATAC) hydrogels. The data are presented as the fractional mass change [31], which is defined as $F_m=(m_{temp}-m_{dry})/(m_{25}-m_{dry})$, the subscripts temp, dry, and 25 refer to the mass of the hydrogel at a given temp, dried, and at 25 °C, respectively. Therefore, F_m represents the fractional change in hydrogel water mass.

The fractional mass change behavior for the two hydrogel types exhibits some gross differences. The anionically charged, AAc-containing hydrogels exhibit a more gradual change in F_m with temperature increases than do the cationically charged, ATAC-containing hydrogels. Specifically, the native p(NIPAm-*co*-ATAC) drop precipitously in F_m, falling below 0.20 by 35 °C. The native p(NIPAm-*co*-AAc) hydrogels, on the other hand, exhibit a more gradual decrease in F_m, not reaching the 0.20 level until temperatures at or above 40 °C. These differences in behavior again likely relate to different properties of the co-monomers including the presence of greater charge within the AAc-containing hydrogels. Co-monomers are well known to alter the shape of the phase transition curve, even enabling the change from a discontinuous to continuous phase transition [14, 32].

Despite these differences in phase behavior between the two hydrogel types, many similarities also exist. One such similarity is the independence of phase transition behavior on the type and concentration of cross-linker present in the native hydrogel—the solid symbols and lines in Fig. 6. No general trend in the change of F_m with temperature is seen for either p(NIPAm-*co*-AAc) (a) or p(NIPAm-*co*-ATAC) (b). Rather, the native hydrogel's phase transition curves cluster together. However, the same behavior is not seen after the in situ synthesis of gold nanostructures within the hydrogel matrix. The data for gold-containing hydrogels (open symbols and dashed lines in Fig. 6) that also contain CBAm at any concentration have shifted to higher phase transition temperatures. The 1.75M/1.75C and 3.50M/3.50C p(NIPAm-*co*-AAc) hydrogels (Fig. 6a) do not have a fractional mass that falls below 0.20 until 45 °C—a change of >5 °C from the same composition native hydrogels. Similarly, all CBAm-containing p(NIPAm-*co*-ATAC) hydrogels with gold nanostructures do not reach an F_m value of 0.20 until 37.5 °C, approximately 2.5 °C higher than the native hydrogels with the same cross-linkers. Both 3.50M/0.00C hydrogels, which lack the CBAm cross-linker, exhibit different behavior. These gold-containing hydrogels have phase transition curves at the same (p(NIPAm-*co*-AAc)) or slightly lower (p(NIPAm-*co*-ATAC)) temperatures than their native counterparts.

The influence on phase transition behavior of gold introduction into CBAm-containing hydrogels was observed previously in the p(NIPAm) system [19]. Trends seen in that study parallel those observed with the NIPAm polymers containing either AAc or ATAC co-monomers in the present work. We attribute the shift to higher temperatures in F_m curves following gold nanostructure formation in hydrogels cross-linked with CBAm to two factors. First, the smaller, more well-separated gold nanostructures created within the CBAm hydrogels, which are supported by UV–vis spectra in Fig. 3, would result in greater nanoparticle surface area. These nanostructure surfaces are known to possess residual charge, often imparted by the stabilizing agent bound to the particle surface [33]. A second factor is the previously described oxidation of disulfide bridges to charged sulfonate groups, leading to reduced cross-linking within the hydrogel. Together, these two factors also result in greater osmotic swelling of the hydrogel through the Donnan effect [20, 28].

Conclusion

These studies reveal that a number of parameters can be altered to tune the properties of NIPAm-based hydrogels containing gold nanostructures. The presence of cationic or anionic co-monomers in the hydrogel decreases or increases, respectively, the number of gold nanostructures formed within

the hydrogel matrix. The use of a disulfide-bridged cross-linking agent has significant influence on the properties of the nanostructures created within the hydrogel—higher concentrations leading to the formation of smaller, more isolated nanostructures as indicated by UV–visible spectroscopy. The thermoresponsive behavior of the composite is also dependent on the concentration of the cleavable cross-linking agent. These synthetic parameters create flexibility that may be key to realizing the potential of hydrogel–metal nanostructure composites.

Acknowledgments The authors thank Ms. Katherine E. Wagner and Ms. Jessica R. Bell for some methods development with the p(NIPAm-*co*-ATAC) and p(NIPAm-*co*-AAc) systems and Ms. Munzarin F. Qayyum for feedback on the manuscript. This work was partially supported by donors of The American Chemical Society Petroleum Research Fund through Grant PRF42899-GB10, by the National Science Foundation (grant CHE-0353813), and by the Department of Chemistry and Brachman Hoffman Program, Wellesley College.

References

1. Yang X, Pan X, Blyth J, Lowe CR (2008) Biosens Bioelectron 23:899
2. Matsui J, Akamatsu K, Hara N, Miyoshi D, Nawafune H, Tamaki K, Sugimoto N (2005) Anal Chem 77:4282
3. Sershen SR, Westcott SL, Halas NJ, West JL (2002) Appl Phys Lett 80:4609
4. Sershen SR, Westcott SL, West JL, Halas NJ (2001) Appl Phys B: Lasers Opt 73:379
5. AN Shipway, I Willner (2001) Chem Commun, Cambridge, UK, p 2035
6. Murthy PSK, Mohan YM, Varaprasad K, Sreedhar B, Raju KM (2008) J Colloid Interface Sci 318:217
7. Thomas V, Yallapu MM, Sreedhar B, Bajpai SK (2007) J Colloid Interface Sci 315:389
8. Shiotani A, Mori T, Niidome T, Niidome Y, Katayama Y (2007) Langmuir 23:4012
9. Lee W-F, Chiu R-J (2002) Mater Sci Eng C C20:161
10. Bikram M, Gobin AM, Whitmire RE, West JL (2007) J Control Release 123:219
11. Jiang XW, Xiong DA, An YL, Zheng PW, Zhang WQ, Shi LQ (2007) J Polym Sci Part A: Polym Chem 45:2812
12. Mohan YM, Lee K, Premkumar T, Geckeler KE (2007) Polymer 48:158
13. Thomas V, Namdeo M, Mohan YM, Bajpai SK, Bajpai M (2008) J Macromol Sci Part A: Pure Appl Chem 45:107
14. Schild HG (1992) Prog Polym Sci 17:163
15. Serizawa T, Uemura M, Kaneko T, Akashi M (2002) J Polym Sci Part A: Polym Chem 40:3542
16. Kabra BG, Gehrke SH (1991) Polymer Commun 32:322
17. Shibayama M, Norisuye T, Nomura S (1996) Macromolecules 29:8746
18. Kim J-H, Lee TR (2007) Langmuir 23:6504
19. Pong FY, Lee M, Bell JR, Flynn NT (2006) Langmuir 22:3851
20. Wang C, Flynn NT, Langer R (2004) Adv Mater (Weinh) 16:1074
21. Kim SJ, Lee CK, Lee YM, Kim SI (2003) J Appl Polym Sci 90:3032
22. Petrovic SC, Zhang W, Ciszkowska M (2000) Anal Chem 72:3449
23. Brown KR, Walter DG, Natan MJ (2000) Chem Mater 12:306
24. Matsuo ES, Tanaka T (1988) J Chem Phys 89:1695
25. Blatchford CG, Campbell JR, Creighton JA (1982) Surf Sci 120:435
26. Sheeney-Haj-Ichia L, Sharabi G, Willner I (2002) Adv Funct Mater 12:27
27. Huglin MB, Liu Y, Velada JL (1997) Polymer 38:5785
28. Katchalsky A, Lifson S, Eisenberg H (1951) J Polym Sci 7:571
29. Plunkett KN, Kraft ML, Yu Q, Moore JS (2003) Macromolecules 36:3960
30. Gehrke SH, Palasis M, Akhtar MK (1992) Polym Int 29:29
31. Makino K, Hiyoshi J, Ohshima H (2000) Colloids Surf B 19:197
32. Hirotsu S, Hirokawa Y, Tanaka T (1987) J Chem Phys 87:1392
33. Schmid G (2001) In: Klabunde KJ (ed) Nanoscale Materials in Chemistry. Wiley, New York, p 15